Research Article Vol. 4, No. 5 / May 2017 / Optica 520

Extreme ultraviolet vector beams driven by infrared lasers

Carlos Hernández-García,[1,*] Alex Turpin,[2,3] Julio San Román,[1] Antonio Picón,[1] Rokas Drevinskas,[4] Ausra Cerkauskaite,[4] Peter G. Kazansky,[4] Charles G. Durfee,[5] and Íñigo J. Sola[1]

[1]Grupo de Investigación en Aplicaciones del Láser y Fotónica, Departamento de Física Aplicada, University of Salamanca, E-37008 Salamanca, Spain
[2]Universitat Autònoma de Barcelona, Cerdanyola del Vallès, E-08193 Barcelona, Spain
[3]Center of Advanced European Studies and Research, 53175 Bonn, Germany
[4]Optoelectronics Research Centre, University of Southampton, UK
[5]Department of Physics, Colorado School of Mines, Golden, Colorado 80401, USA
*Corresponding author: carloshergar@usal.es

Received 2 February 2017; revised 31 March 2017; accepted 1 April 2017 (Doc. ID 286062); published 4 May 2017

Vector beams, beams with a non-uniform state of polarization, have become an indispensable tool in many areas of science and technology. Harnessing topological light properties paves the way to control and manipulate light–matter interactions at different levels, from the quantum to macroscopic physics. Here we generate tabletop extreme ultraviolet (EUV) vector beams driven by high-order harmonic generation (HHG). Our experimental and theoretical results demonstrate that HHG imprints the polarization state of the fundamental (infrared) beam, ranging from radial to azimuthal, into the higher frequency radiation. Our numerical simulations also demonstrate that the generated high-order harmonic beams can be synthesized into attosecond vector beams in the EUV/soft x-ray regime. Our proposal overcomes the state-of-the-art-limitations for the generation of vector beams far from the visible domain and could be applied in fields such as diffractive imaging, EUV lithography, or ultrafast control of magnetic properties.

OCIS codes: (320.7110) Ultrafast nonlinear optics; (260.7200) Ultraviolet, extreme; (340.7480) X-rays, soft x-rays, extreme ultraviolet (EUV); (260.5430) Polarization.

https://doi.org/10.1364/OPTICA.4.000520

1. INTRODUCTION

The state of polarization of light is often considered as a property independent of the spatio-temporal beam distribution. Using this approach, a light field can be described as $\vec{E}(\vec{r},t) = E(\vec{r},t)\vec{e}_0$, where $\vec{e}_0$ is the light's state of polarization. In this case, $\vec{e}_0$ is uniform along the whole light beam, which is the common case for beams with a linear, elliptical, or circular state of polarization. However, there are scenarios where the polarization state varies from point to point of the light beam, i.e., $\vec{e}_0 = \vec{e}_0(\vec{r},t)$. Light beams with spatially variant polarization, $\vec{e}_0 = \vec{e}_0(\vec{r})$, are known as vector beams. In recent years, there has been an increased interest in the generation of vector beams due to the novel effects they present and their particular interaction with matter, making them essential tools in different areas of science and technology [1]. Light beams with radial and azimuthal polarizations are the paradigm of vector beams. On one hand, radial vector beams are especially interesting due to the non-vanishing longitudinal electric field component present in tightly focusing systems, which allows one to sharply focus light below the diffraction limit [2,3]. This property has been greatly significant in fields such as laser machining [4–7], optimal plasmonic focusing [8], particle acceleration [9,10], and molecular orientation determination [2,11]. Radially polarized vector beams have also been shown to be relevant for the nanolocalization of dielectric particles [12], and the control of the radiation of relativistic electrons [13]. On the other hand, azimuthal vector beams can induce longitudinal magnetic fields with potential applications in spectroscopy and microscopy [14]. In addition, we note that vector beams present other interesting applications in the generation of quantum memories with multiples degrees of freedom [15], enhanced optical trapping [16], and polarization-dependent measurements in atomic systems [17]. They have also been used in fundamental science to demonstrate an optical analog to the spin Hall effect [18], to extend the concept of Pancharatnam–Berry phase [19], to observe an optical Möbius strip [20], and in the entanglement of complex modes both in the quantum [21] and classical [22,23] regimes.

Over the last two decades, high-order harmonic generation (HHG) has been demonstrated as a unique mechanism for the generation of coherent EUV and soft x-ray radiation, in the form of attosecond bursts [24,25]. The underlying physics at the microscopic level can be simply understood by the so-called three-step model [26,27]: An electron is tunnel ionized from an atom or molecule by an intense linearly polarized laser field, then accelerated, and finally driven back to its parent ion, releasing all the energy acquired during the process in the form of high-order

harmonics upon recombination, extending from the EUV to the soft x-ray regimes [28]. From the macroscopic point of view of the HHG process, an infrared laser beam is focused into a gas target, and, if efficient phase-matching conditions are met [29], an EUV/x-ray beam is emitted.

There are different techniques to produce vector beams in the infrared-visible regime. Vector beams presenting cylindrical symmetry, i.e., cylindrical vector beams, have been demonstrated by the coherent addition of two orthogonally polarized Hermite–Gauss beams [1,30], by means of both uniaxial [5,31] and biaxial [32] crystals, using circular multilayer polarizing grating end mirrors [33], with azimuthally dependent half-waveplates (s-waveplates) [34], by combining two spatial light modulators [35], with optical fibers [36], by means of electrically-tuned q-plates [37], and with a glass cone [38]. Non-cylindrically symmetric vector beams have been reported using c-cut uniaxial crystals [39], conical refraction in biaxial crystals [40], with q-plates [41], and by transforming a Laguerre–Gauss beam with a half-waveplate and a π cylindrical lens mode converter [19]. However, the spectral limitations of these generation techniques based on linear optics prevent the efficient generation of vector beams in the extreme-ultraviolet (EUV) and x-ray regimes, which would further extend the applications mentioned in the previous paragraph down to the nanometric scale. One of the most valuable aspects of HHG is that the properties of the EUV/x-ray harmonics can be controlled through proper modifications of the driving beam, thus avoiding the use of inefficient optical devices in the EUV/x-ray regime to control the beam properties. For instance, not only the spatio-temporal properties of the driving field are imprinted in the harmonic beam, but also the mechanical properties involving orbital angular momentum (OAM) and/or spin (polarization). On one hand, EUV beams with spatial phase twist have been recently generated through OAM conservation [42–44], conveying the synthetization of attosecond helical beams [42,45,46]. Regarding the polarization state of the harmonics, although the HHG conversion efficiency drops quickly with the increase of the ellipticity of the driving field [47], different techniques have been recently developed to generate elliptically and circularly polarized harmonics through spin angular momentum conservation [48–52]. As a result, attosecond pulses from elliptical [53,54] to purely circular polarization [55] are predicted to be produced.

In this work, we overcome the existing limitations for the generation of EUV/x-ray vector beams by transferring the complex structure of the infrared vector beam through high-order harmonic generation. We use an s-waveplate to generate infrared driving vector beams (from radial to azimuthal) that are upconverted to shorter wavelength radiation. Our numerical simulations are in excellent agreement with the experimental results, which allows us to predict that harmonic vector beams can be synthesized into attosecond vector beams.

The driving beam, a linearly polarized femtosecond infrared pulse, is converted into a radial/azimuthal vector beam using an s-waveplate [34]. The s-waveplate is a super-structured space variant waveplate that converts linear to radial or azimuthal polarization, depending on the polarization angle of the incident beam (see Figs. 1(a) and 1(b), respectively). To characterize the resulting vector beam we place: a half-waveplate before the s-waveplate to control the input beam polarization direction, and a vertical linear polarizer after the s-waveplate to analyze the generated beam. In Fig. 1(c) we plot the measured spatial intensity distribution observed after the analyzer for different angles (α) of the half-waveplate. We observe that for $\alpha = 0°$ we obtain a radial vector beam distribution, while for $\alpha = 45°$ we obtain an azimuthal vector beam. Once the IR vector beam is properly selected, we generate high-order harmonics by focusing the beam into an argon gas jet, as sketched in Figs. 1(a) and 1(b). The resulting harmonic vector beam is detected in the far-field.

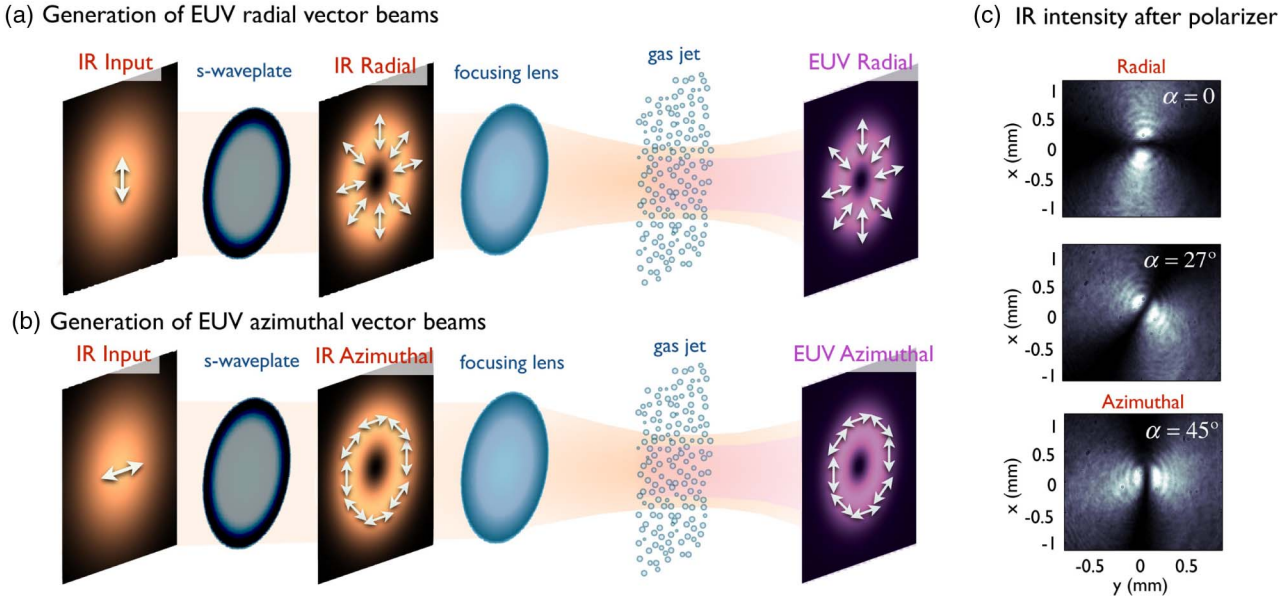

Fig. 1. Scheme for the generation of (a) EUV radial and (b) azimuthal vector beams. A vertically, or horizontally, linearly polarized IR beam is converted into a radial, or azimuthal, IR beam by an s-waveplate, respectively. The resulting vector beam is focused into a gas jet, where each atom interacts with the local IR field, emitting linearly polarized harmonics in the EUV/x-ray regime. Upon propagation, the far-field high-order harmonics are emitted in the form of (a) radial or (b) azimuthal vector beams. (c) Spatial intensity distribution of the IR vector beam generated in the lab with the s-waveplate, after passing through a vertical linear polarizer (the analyzer). With the help of a half-waveplate (axis angle α) placed before the s-waveplate, the input IR linear polarization is varied from vertical ($\alpha = 0°$) to horizontal ($\alpha = 45°$).

2. RESULTS

A. Theoretical and Experimental Generation of Harmonic Vector Beams

To study the generation of EUV/x-ray vector beams through HHG, we first perform numerical simulations, including propagation through the electromagnetic field propagator [56] (see Section 1 of Supplement 1). In our simulations, we consider the infrared beam as a Laguerre–Gaussian mode ($LG_{1,0}$) without the azimuthal phase (see Section 1 of Supplement 1) with varying spatial polarization. In particular, we have considered radial and azimuthal vector beams with a beam waist $w_0 = 30$ μm. The argon gas jet is modeled by a Gaussian distribution along the y and z dimensions, whose full width at half-maximum (FWHM) is 500 μm, and possesses a constant profile along its axial dimension, x, with a peak density of 10^{17} atoms/cm^3. For the simulations presented below, the laser pulse envelope is assumed to be a sine-squared function of 5.8 cycles (15.2 fs) FWHM, whose amplitude (E_0) is chosen to give a maximum peak intensity at focus of 1.6×10^{14} W/cm^2 at a wavelength of $\lambda = 790$ nm. Longer pulses that are closer to our experimental driver were not implemented due to the high computational time required, and they would not have modified the main results presented in this work.

In Fig. 2 we present the simulated angular intensity profiles of the 17th harmonic (46.5 nm, 26.7 eV, first and third rows) and the 23rd harmonic (34.3 nm, 36.1 eV, second and fourth rows), driven by an IR radial, (a) and (b), and azimuthal, (c) and (d), vector beam. For each harmonic, we show the intensity distribution projected into the vertical and horizontal polarization, and the sum of both components. As it can be appreciated, the state of polarization of each harmonic is that of the driving beam, i.e., both HHG and the harmonic phase-matching preserve the generation of radial and azimuthal vector EUV beams. With respect to the beam profile, one can clearly appreciate that the on-axis nodal point of the fundamental beam is preserved in the far-field emission of harmonics. Recently, it was shown that the far-field emission of harmonics generated with an annular beam intensity profile with linear polarization carrying OAM also leads to an on-axis dark point due to a phase singularity present in light beams carrying integer OAM [42–46,57]. In this work the annular beam intensity does not exhibit OAM, but is radially or azimuthally polarized, i.e., it possesses a polarization singularity that manifests as the on-axis nodal point both at the fundamental beam and high-order

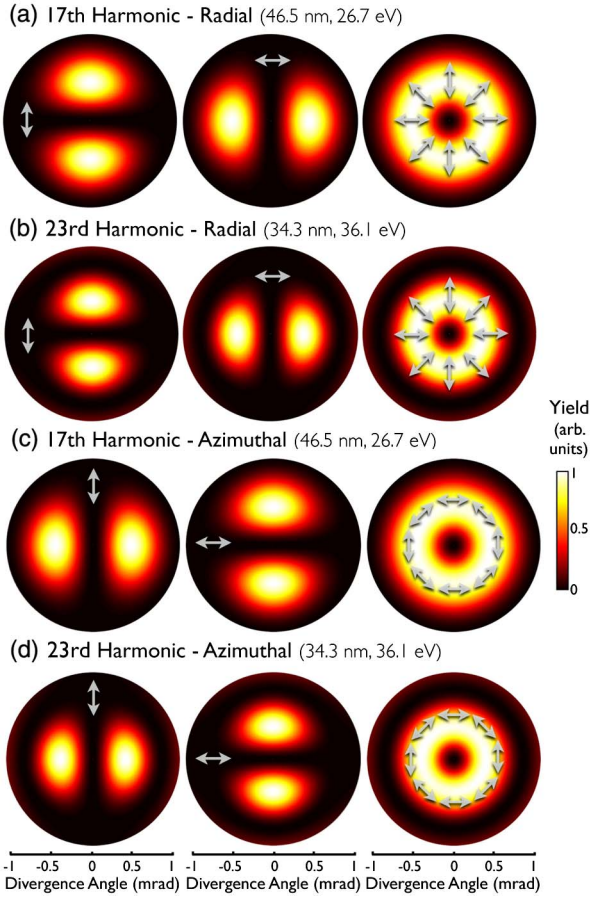

Fig. 2. Angular intensity plots showing the spatial far-field profile of the 17th harmonic (46.5 nm, 26.7 eV, first and third rows) and the 23rd harmonic (34.3 nm, 36.1 eV, second and fourth), driven by a radial, (a) and (b), and azimuthal, (c) and (d), IR vector beam. For each case, we show (from left to right) the vertical and horizontal polarization projections, and the sum of both components. It can be observed that each harmonic is emitted as a radial or azimuthal vector beam, according to the driving beam.

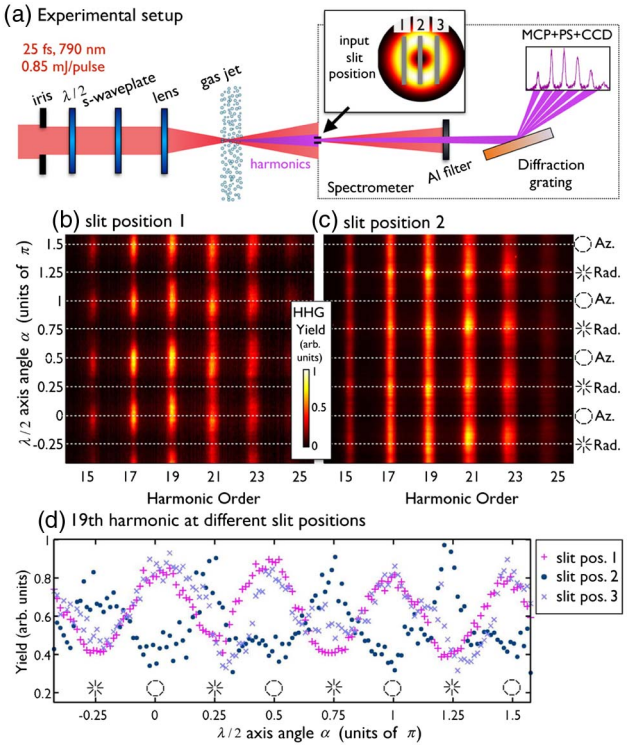

Fig. 3. (a) Experimental setup. A Gaussian linearly polarized IR beam is converted into a vector beam after passing through a half-waveplate and the s-waveplate. High-order harmonics are generated after focusing the beam into an Ar gas jet. The spectrometer input slit is placed at three different spatial positions of the harmonic beam, as indicated on the inset (note that the inset background is taken from Fig. 2). An aluminum filter is used to remove the IR beam, and the harmonics are separated by means of a diffraction grating. The HHG spectra recorded at (b) slit position 1 and (c) slit position 2 is shown as a function of the half-waveplate angle axis (α). The $\pi/2$ periodicity allows us to identify the cases where the vector beam is radially or azimuthally polarized. In plot (d) we show the 19th harmonic signal as a function of α for the three slit positions selected. The yield at each position is normalized separately.

harmonics. The output of the s-waveplate may be considered to be a superposition of radial modes, all of which share the polarization state that forces the on-axis singularity.

In Fig. 3 we present the experimental results. The setup, which is detailed in Section 2 of Supplement 1, is shown in Fig. 3(a). The laser system (Femtopower HE PRO CEP system) delivers linearly polarized 25 fs pulses at a central wavelength of 790 nm, operating at a 1 kHz repetition rate and 0.85 mJ/pulse. A half-waveplate placed before the s-waveplate, allows us to select the input polarization direction, and thus the polarization distribution of the IR vector beam that is focused (focal length 30 cm) into an argon gas jet to drive harmonics. An iris was placed before the half-waveplate to optimize the harmonic phase-matching conditions [58]. The harmonic radiation enters into a Rowland-circle-type spectrometer through a thin slit. In this work, we have horizontally displaced the EUV beam through the entrance slit to characterize different parts of the EUV beam, as depicted in the inset of Fig. 3(a). The diffraction grating in the spectrometer acts as a EUV polarizer, allowing us to characterize the harmonic polarization. To this end, we first characterized the spectrometer response to different linear polarization orientations by using the half-waveplate before the lens (without the s-waveplate), rotated at different angles, obtaining a maximum signal for vertical polarization (s-polarization) and a minimum for horizontal (p-polarization), as depicted in Fig. S1 in Supplement 1. Although other more sophisticated EUV polarizers could be used [59], the different efficiency of both polarization directions already allows us to characterize the EUV vector beams.

In Figs. 3(b) and 3(c) we present the harmonic intensity measured as a function of the half-waveplate axis angle (α), for the radiation entering through the slit position 1 (at the left edge of the beam) and slit position 2 (at the center of the beam), respectively. By rotating the half-waveplate axis, we generate all kinds of vector beams from radial to azimuthal. It can be observed that when α is 0, 0.5π, π, and 1.5π, the HHG signal presents a maximum at slit position 1 (b), while a minimum at slit position 2 (c), indicating that the EUV presents azimuthal polarization. On the other hand, the behavior is reversed at α equal to -0.25π, 0.25π, 0.75π, and 1.25π, indicating the generation of an EUV radial beam.

The 19th harmonic signal as a function of the half-waveplate axis angle (α) is plotted in the panel (d) at the three slit positions indicated in panel (a): pink plus signs for the left part of the beam (slit position 1), blue points for the central part (slit position 2), and purple crosses for the right part (slit position 3). We observe that the angle dependence for slit positions 1 and 3 is very similar, and completely out of phase with slit position 2, thus demonstrating that the 19th harmonic beam has all polarization distributions from radial to azimuthal. The experimental results are in excellent agreement with the theoretical simulations, showing that not only radial an azimuthal EUV beams are generated, but all the intermediate polarization states between these two extreme cases.

One of the most interesting properties of radially polarized beams is that they present a strong longitudinal electric field when tightly focused. In our HHG experiment, we have selected a loose focusing geometry (focal length of 30 cm, giving a maximum numerical aperture of NA = 0.04) for which the longitudinal electric field is negligible [1,60]. Note that harmonic phase-matching conditions would be modified in tighter focusing geometries where the driving field presents a longitudinal component, leading to modifications in the far-field harmonic profile [61].

B. Synthesis of Attosecond Vector Beams

High-order harmonics are naturally emitted in the form of attosecond pulses. Our simulations show that harmonic vector beams are also emitted as attosecond vector beams (Fig. 4). For this to happen, it is essential that several harmonics overlap spatially. In Fig. 4(a) we show the far-field divergence of the several x-polarized harmonics (from the 17th to the 23rd) when driven by an IR radial vector beam. We observe that there is a range of divergence angles in which these harmonics overlap with comparable intensity. Hence, our numerical simulations show that:

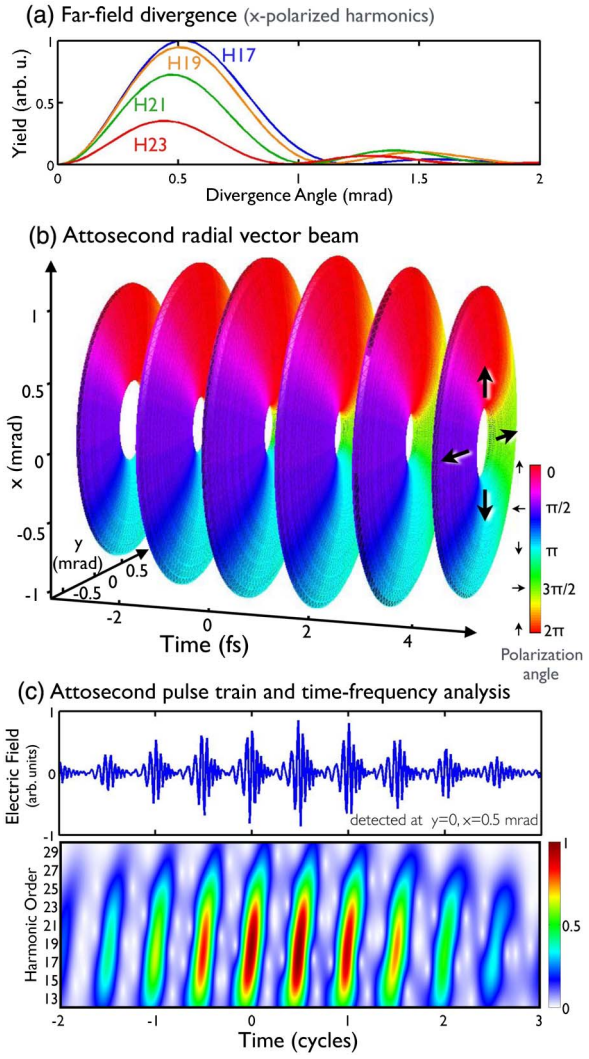

Fig. 4. Attosecond vector beams. (a) Far-field divergence of the 17th (blue), 19th (orange), 21st (green), and 23rd (red) harmonics with x-polarization detected at $y = 0$ mrad. (b) Isosurface representation of the attosecond radial vector beam resulting after performing the Fourier transform of the high-order harmonics presented in Fig. 3(b). The color scale represents the polarization azimuth, as indicated by the arrows. (c) Attosecond pulse train (top) and time-frequency analysis (bottom) detected at $y = 0$, $x = 0.5$ mrad. The positive slope of the time-frequency structures indicates that the attosecond pulses are emitted with positive chirp.

(i) The polarization structure of different harmonics is the same for all the harmonic orders, and (ii) There is a wide range of observation angles where different high-order harmonics overlap. These two results allow us to coherently sum several harmonics to synthesize attosecond pulses. In Fig. 4(b) we show the isosurface attosecond radial vector beam obtained from the Fourier transform of the coherent integration of the high-order harmonics emitted in an argon gas jet (same parameters as in Fig. 2). The higher-order harmonics above the 11th have been selected by considering the transmission through an aluminum filter. The color scale shows the direction of the polarization at each spatial position of the beam. As it can be observed, each attosecond pulse within the train exhibits a radially polarized spatial distribution, mimicking that of the IR fundamental beam. In Fig. 4(c) we show the x-polarized attosecond pulse train (top) and time-frequency analysis (bottom) detected at $y = 0$, $x = 0.5$ mrad. The time-frequency analysis shows the temporal intervals when the high-order harmonics are emitted. The positive slope indicates that the so-called short trajectories are phase-matched, imprinting a positive chirp in the attosecond pulses. The positive chirp, together with the different divergence of the harmonics [shown in Fig. 4(a)], explains the conical shape of attosecond radial vector beam presented in Fig. 4(b). Although here we only showed the attosecond vector beam with radial polarization, attosecond beams with polarization from radial to azimuthal can be obtained through adequate synthesis of the harmonic vector beams presented in Section 2.A.

3. DISCUSSION

We have demonstrated, both experimentally and theoretically, the generation of coherent vector beams in the EUV regime driven by HHG. To do so, a fs radially polarized vector beam obtained with a s-waveplate in the infrared domain has been focused into an argon gas target at standard experimental conditions. The atoms within the target emit EUV radiation coherently providing that efficient phase-matching conditions are met. With this physical scenario, we have shown that the non-homogeneous polarization nature of the fundamental beam is transferred to the HHG beam, i.e., vector beams of both radial and azimuthal polarization in the EUV domain are obtained. We recall that HHG offers a unique opportunity for the generation of vector beams at very short wavelengths, unreachable with other frequency upconversion techniques, such as second- and third-harmonic generation in crystals, since in these techniques the state of polarization of the fundamental beam is destroyed during the nonlinear process. Note that higher-photon energies up to the soft x-ray regime can be obtained if longer, mid-infrared [28], or shorter, ultraviolet [62] wavelengths were used. We do not expect the fundamental physics presented here to be different in those two scenarios.

We have demonstrated theoretically that EUV attosecond vector beams can be produced by means of HHG. Note that although we have reported attosecond vector beams where the spatial polarization distribution is maintained from pulse to pulse, gating schemes [63] could be applied to harness the time-dependent polarization profile of these beams, and thus to produce vector beams that vary from radial to azimuthal polarization in the time domain. Similar schemes could be used to isolate a single attosecond pulse with the desired polarization distribution.

We also note that radially and azimuthally polarized beams are the natural (albeit nearly degenerate) modes of cylindrical waveguides [64]. By coupling the vector beams into capillary waveguides, phase matching and an increased interaction length should allow for the generation of more harmonic flux than obtained in the present experiment. Moreover, still higher yield is anticipated considering that the peak intensity is away from the optical axis. The harmonic amplitude is known to scale with the ~4th power of the fundamental amplitude for the high-order harmonics generated in argon (see Supplemental Material at [44]). A simple integration of $LG_{0,0}$ and $LG_{1,0}$ mode profiles with same peak intensity, weighted by the 4th power harmonic intensity yield, shows that the effective source volume is more than 5× greater for the higher mode, in agreement with our quantum HHG simulations (see Section 3 of Supplement 1). Thus, we anticipate that gas-filled capillary waveguides, which were used to efficiently phase-match soft x-ray harmonics [28], are the perfect candidates to generate soft x-ray vector beams through HHG.

To our knowledge this is the first time that vector beams in the EUV regime have been produced in a tabletop setup, and most important, in the form of attosecond-to-femtosecond pulses that are perfectly synchronized to the driving laser. Vector beams already offer many applications in the optical domain, where, in particular, radial vector beams exhibit the sharpest possible focus. This, combined with the state-of-the-art EUV/X-ray focusing techniques already allowing for focal spots as small as 15 nm [65], will bring the application of vector beams to the nanometric scale, especially in areas such as ultrafast diffraction imaging [25,66] and EUV lithography [67,68].

On the other hand, the longitudinal magnetic field created at the center of tightly focused azimuthal vector beams presents promising applications in magnetic spectroscopy and microscopy [14]. The generation of ultrashort EUV/x-ray azimuthal vector beams conveys a revolutionary tool to be applied in nanomagnetics, due to their potential to generate ultrafast electronic currents in the nanoscale. Ultrafast charge currents can induce magnetic fields that steer the properties of magnetic nanoparticles [69]. We envision a unique opportunity to tailor magnetic domains in the femtosecond-to-attosecond timescales using EUV/x-ray vector beams.

Funding. Research Executive Agency (REA) (328334); Consejería de Educación, Junta de Castilla y León (SA046U16); Ministerio de Economía y Competitividad (MINECO) (FIS2011-23719, FIS2013-44174-P, FIS2015-71933-REDT, FIS2016-75652-P); Ministerio de Educación, Cultura y Deporte (MECD) (AP2010-2310); Consell Català de Recerca i Innovació (SGR2014-1639); Air Force Office of Scientific Research (AFOSR) (FA9550-16-1-0121); National Science Foundation (NSF) (1619518); Engineering and Physical Sciences Research Council (EPSRC) (EP/M029042/1); Horizon 2020 Framework Programme (H2020) (702565).

Acknowledgment. We acknowledge Professor Luis Plaja for his fruitful discussions. We also acknowledge support from Centro de Láseres Pulsados (CLPU) and the Max Planck Society.

See Supplement 1 for supporting content.

REFERENCES

1. Q. Zhan, "Cylindrical vector beams: from mathematical concepts to applications," Adv. Opt. Photon. **1**, 1–57 (2009).

2. L. Novotny, M. R. Beversluis, K. S. Youngworth, and T. G. Brown, "Longitudinal field modes probed by single molecules," Phys. Rev. Lett. **86**, 5251–5254 (2001).
3. R. Dorn, S. Quabis, and G. Leuchs, "Sharper focus for a radially polarized light beam," Phys. Rev. Lett. **91**, 233901 (2003).
4. M. Meier, V. Romano, and T. Feurer, "Material processing with pulsed radially and azimuthally polarized laser radiation," Appl. Phys. A **86**, 329–334 (2007).
5. C. Hnatovsky, V. Shvedov, W. Krolikowski, and A. Rode, "Revealing local field structure of focused ultrashort pulses," Phys. Rev. Lett. **106**, 123901 (2011).
6. J. J. J. Nivas, S. He, A. Rubano, A. Vecchione, D. Paparo, L. Marrucci, R. Bruzzese, and S. Amoruso, "Direct femtosecond laser surface structuring with optical vortex beams generated by a q-plate," Sci. Rep. **5**, 17929 (2015).
7. R. Drevinskas, J. Zhang, M. Beresna, M. Gecevicius, A. G. Kazanskii, Y. P. Svirko, and P. G. Kazansky, "Laser material processing with tightly focused cylindrical vector beams," Appl. Phys. Lett. **108**, 221107 (2016).
8. Q. Zhan, "Evanescent Bessel beam generation via surface plasmon resonance by radially polarized beam," Opt. Lett. **31**, 1726–1728 (2006).
9. Y. I. Salamin, Z. Harman, and C. H. Keitel, "Direct high-power laser acceleration of ions for medical applications," Phys. Rev. Lett. **100**, 155004 (2008).
10. V. Marceau, C. Varin, T. Brabec, and M. Piché, "Femtosecond 240-keV electron pulses from direct laser acceleration in a low-density gas," Phys. Rev. Lett. **111**, 224801 (2013).
11. N. Karedla, S. C. Stein, D. Hähnel, I. Gregor, A. Chizhik, and J. Enderlein, "Simultaneous measurement of the three-dimensional orientation of excitation and emission dipoles," Phys. Rev. Lett. **115**, 173002 (2015).
12. S. Roy, K. Ushakova, Q. van den Berg, S. F. Pereira, and H. P. Urbach, "Radially polarized light for detection and nanolocalization of dielectric particles on a planar substrate," Phys. Rev. Lett. **114**, 103903 (2015).
13. L. Schächter and W. D. Kimura, "Vacuum channeling radiation by relativistic electrons in a transverse field of a laser-based Bessel beam," Phys. Rev. Lett. **114**, 195501 (2015).
14. C. Guclu, M. Veysi, and F. Capolino, "Photoinduced magnetic nanoprobe excited by an azimuthally polarized vector beam," ACS Photon. **3**, 2049–2058 (2016).
15. V. Parigi, V. D'Ambrosio, C. Arnold, L. Marrucci, F. Sciarrino, and J. Laurat, "Storage and retrieval of vector beams of light in a multiple-degree-of-freedom quantum memory," Nat. Commun. **6**, 7706 (2015).
16. V. Salakhutdinov, M. Sondermann, L. Carbone, E. Giacobino, A. Bramati, and G. Leuchs, "Optical trapping of nanoparticles by full solid-angle focusing," Optica **3**, 1181–1186 (2016).
17. F. K. Fatemi, "Cylindrical vector beams for rapid polarization-dependent measurements in atomic systems," Opt. Express **19**, 25143–25150 (2011).
18. M. Neugebauer, P. Banzer, T. Bauer, S. Orlov, N. Lindlein, A. Aiello, and G. Leuchs, "Geometric spin Hall effect of light in tightly focused polarization-tailored light beams," Phys. Rev. A **89**, 013840 (2014).
19. G. Milione, S. Evans, D. A. Nolan, and R. R. Alfano, "Higher order Pancharatnam–Berry phase and the angular momentum of light," Phys. Rev. Lett. **108**, 190401 (2012).
20. T. Bauer, P. Banzer, E. Karimi, S. Orlov, A. Rubano, L. Marrucci, E. Santamato, R. W. Boyd, and G. Leuchs, "Observation of optical polarization Möbius strips," Science **347**, 964–966 (2015).
21. R. Fickler, R. Lapkiewicz, S. Ramelow, and A. Zeilinger, "Quantum entanglement of complex photon polarization patterns in vector beams," Phys. Rev. A **89**, 060301(R) (2014).
22. E. Karimi and R. W. Boyd, "Classical entanglement?" Science **350**, 1172–1173 (2015).
23. M. McLaren, T. Konrad, and A. Forbes, "Measuring the nonseparability of vector vortex beams," Phys. Rev. A **92**, 023833 (2015).
24. F. Krausz and M. Ivanov, "Attosecond physics," Rev. Mod. Phys. **81**, 163–234 (2009).
25. J. Miao, T. Ishikawa, I. K. Robinson, and M. M. Murnane, "Beyond crystallography: diffractive imaging using coherent x-ray light sources," Science **348**, 530–535 (2015).
26. K. J. Schafer, B. Yang, L. F. DiMauro, and K. C. Kulander, "Above threshold ionization beyond the high harmonic cutoff," Phys. Rev. Lett. **70**, 1599–1602 (1993).
27. P. B. Corkum, "Plasma perspective on strong field multiphoton ionization," Phys. Rev. Lett. **71**, 1994–1997 (1993).
28. T. Popmintchev, M. Chen, D. Popmintchev, P. Arpin, S. Brown, S. Ališauskas, G. Andriukaitis, T. Balčiunas, O. Mücke, A. Pugzlys, A. Baltuška, B. Shim, S. E. Schrauth, A. Gaeta, C. Hernández-García, L. Plaja, A. Becker, A. Jaroń-Becker, M. M. Murnane, and H. C. Kapteyn, "Bright coherent ultrahigh harmonics in the keV X-ray regime from mid-infrared femtosecond lasers," Science **336**, 1287–1291 (2012).
29. M. B. Gaarde, J. L. Tate, and K. J. Schafer, "Macroscopic aspects of attosecond pulse generation," J. Phys. B **41**, 132001 (2008).
30. V. G. Niziev, R. S. Chang, and A. V. Nesterov, "Generation of inhomogeneously polarized laser beams by use of a Sagnac interferometer," Appl. Opt. **45**, 8393–8399 (2006).
31. V. G. Shvedov, C. Hnatovsky, N. Shostka, and W. Krolikowski, "Generation of vector bottle beams with a uniaxial crystal," J. Opt. Soc. Am. B **30**, 1–6 (2013).
32. C. F. Phelan, J. F. Donegan, and J. G. Lunney, "Generation of a radially polarized light beam using internal conical diffraction," Opt. Express **19**, 21793–21802 (2011).
33. M. A. Ahmed, A. Voss, M. M. Vogel, and T. Graf, "Multilayer polarizing grating mirror used for the generation of radial polarization inYb:YAG thin-disk lasers," Opt. Lett. **32**, 3272–3274 (2007).
34. M. Beresna, M. Gecevicius, P. G. Kazansky, and T. Gertus, "Polarization sensitive elements fabricated by femtosecond laser nanostructuring of glass," Opt. Mater. Express **1**, 783–795 (2011).
35. M. R. Beversluis, L. Novotny, and S. J. Stranick, "Programmable vector point-spread function engineering," Opt. Express **14**, 2650–2656 (2006).
36. T. Hirayama, Y. Kozawa, T. Nakamura, and S. Sato, "Generation of a cylindrically symmetric, polarized laser beam with narrow linewidth and fine tunability," Opt. Express **14**, 12839–12845 (2006).
37. V. D'Ambrosio, F. Baccari, S. Slussarenko, L. Marrucci, and F. Sciarrino, "Arbitrary, direct and deterministic manipulation of vector beams via electrically-tuned q-plates," Sci. Rep. **5**, 7840 (2015).
38. N. Radwell, R. D. Hawley, J. B. Götte, and S. Franke-Arnold, "Achromatic vector vortex beams from a glass cone," Nat. Commun. **7**, 10564 (2015).
39. T. A. Fadeyeva, V. G. Shvedov, Y. V. Izdebskaya, A. V. Volyar, E. Brasselet, D. N. Neshev, A. S. Desyatnikov, W. Krolikowski, and Y. S. Kivshar, "Spatially engineered polarization states and optical vortices in uniaxial crystals," Opt. Express **18**, 10848–10863 (2010).
40. A. Turpin, Y. V. Loiko, A. Peinado, A. Lizana, T. K. Kalkandjiev, J. Campos, and J. Mompart, "Polarization tailored novel vector beams based on conical refraction," Opt. Express **23**, 5704–5715 (2015).
41. Y. S. Rumala, G. Milione, T. A. Nguyen, S. Pratavieira, Z. Hossain, D. Nolan, S. Slussarenko, E. Karimi, L. Marrucci, and R. R. Alfano, "Tunable supercontinuum light vector vortex beam generator using a q-plate," Opt. Lett. **38**, 5083–5086 (2013).
42. C. Hernández-García, A. Picón, J. San Román, and L. Plaja, "Attosecond extreme ultraviolet vortices from high-order harmonic generation," Phys. Rev. Lett. **111**, 083602 (2013).
43. G. Gariepy, J. Leach, K. T. Kim, T. J. Hammond, E. Frumker, R. W. Boyd, and P. B. Corkum, "Creating high-harmonic beams with controlled orbital angular momentum," Phys. Rev. Lett. **113**, 153901 (2014).
44. L. Rego, J. San Román, A. Picón, L. Plaja, and C. Hernández-García, "Nonperturbative twist in the generation of extreme-ultraviolet vortex beams," Phys. Rev. Lett. **117**, 163202 (2016).
45. C. Hernández-García, J. San Román, L. Plaja, and A. Picón, "Quantum-path signatures in attosecond helical beams driven by optical vortices," New J. Phys. **17**, 093029 (2015).
46. R. Géneaux, A. Camper, T. Auguste, O. Gobert, J. Caillat, R. Taïeb, and T. Ruchon, "Synthesis and characterization of attosecond light vortices in the extreme ultraviolet," Nat. Commun. **7**, 12583 (2016).
47. P. Dietrich, N. H. Burnett, M. Ivanov, and P. B. Corkum, "High-harmonic generation and correlated two-electron multiphoton ionization with elliptically polarized light," Phys. Rev. A **50**, R3585(R) (1994).
48. H. Eichmann, A. Egbert, S. Nolte, C. Momma, B. Wellegehausen, W. Becker, S. Long, and J. K. McIver, "Polarization-dependent high-order two-color mixing," Phys. Rev. A **51**, R3414(R) (1995).
49. A. Fleischer, O. Kfir, T. Diskin, P. Sidorenko, and O. Cohen, "Spin angular momentum and tunable polarization in high-harmonic generation," Nat. Photonics **8**, 543–549 (2014).
50. D. D. Hickstein, F. J. Dollar, P. Grychtol, J. L. Ellis, R. Knut, C. Hernández-García, C. Gentry, D. Zusin, J. M. Shaw, T. Fan, K. M. Dorney, A. Becker, A. Jaroń-Becker, H. C. Kapteyn, M. M. Murnane, and C. G. Durfee, "Non-collinear generation of angularly isolated circularly polarized high harmonics," Nat. Photonics **9**, 743–750 (2015).

51. T. Fan, P. Grychtol, R. Knut, C. Hernández-García, D. D. Hickstein, D. Zusin, C. Gentry, F. J. Dollar, C. A. Mancuso, C. W. Hogle, O. Kfir, D. Legut, K. Carva, J. L. Ellis, K. M. Dorney, C. Chen, O. G. Shpyrko, E. E. Fullerton, O. Cohen, P. M. Oppeneer, D. B. Milosevic, A. Becker, A. A. Jaron-Becker, T. Popmintchev, M. M. Murnane, and H. C. Kapteyn, "Bright circularly polarized soft X-ray high harmonics for X-ray magnetic circular dichroism," Proc. Natl. Acad. Sci. USA **112**, 14206–14211 (2015).
52. C. Chen, Z. Tao, C. Hernández-García, P. Matyba, A. Carr, R. Knut, O. Kfir, D. Zusin, C. Gentry, P. Grychtol, O. Cohen, L. Plaja, A. Becker, A. Jaron-Becker, H. Kapteyn, and M. Murnane, "Tomographic reconstruction of circularly polarized high-harmonic fields: 3D attosecond metrology," Sci. Adv. **2**, e1501333 (2016).
53. D. B. Milosevic, "Generation of elliptically polarized attosecond pulse trains," Opt. Lett. **40**, 2381–2384 (2015).
54. L. Medišauskas, J. Wragg, H. van der Hart, and M. Y. Ivanov, "Generating isolated elliptically polarized attosecond pulses using bichromatic counterrotating circularly polarized laser fields," Phys. Rev. Lett., **115**, 153001 (2015).
55. C. Hernández-García, C. G. Durfee, D. D. Hickstein, T. Popmintchev, A. Meier, M. M. Murnane, H. C. Kapteyn, I. J. Sola, A. Jaron-Becker, and A. Becker, "Schemes for generation of isolated attosecond pulses of pure circular polarization," Phys. Rev. A **93**, 043855 (2016).
56. C. Hernández-García, J. A. Pérez-Hernández, J. Ramos, E. Conejero Jarque, L. Roso, and L. Plaja, "High-order harmonic propagation in gases within the discrete dipole approximation," Phys. Rev. A **82**, 033432 (2010).
57. M. Zürch, C. Kern, P. Hansinger, A. Dreischuh, and C. Spielmann, "Strong-field physics with singular light beams," Nat. Phys. **8**, 743–746 (2012).
58. C. Hernández-García, I. J. Sola, and L. Plaja, "Signature of the transversal coherence length in high-order harmonic generation," Phys. Rev. A **88**, 043848 (2013).
59. B. Vodungbo, A. Barszczak Sardinha, J. Gautier, G. Lambert, C. Valentin, M. Lozano, G. Iaquaniello, F. Delmotte, S. Sebban, J. Lüning, and P. Zeitoun, "Polarization control of high order harmonics in the EUV photon energy range," Opt. Express **19**, 4346–4356 (2011).
60. K. S. Youngworth and T. G. Brown, "Focusing of high numerical aperture cylindrical-vector beams," Opt. Express **7**, 77–87 (2000).
61. P. Balcou, P. Salieres, A. L'Huillier, and M. Lewenstein, "Generalized phase-matching conditions for high harmonics: the role of field-gradient forces," Phys. Rev. A **55**, 3204–3210 (1997).
62. D. Popmintchev, C. Hernández-García, F. Dollar, C. Mancuso, J. A. Pérez-Hernández, M.-C. Chen, A. Hankla, X. Gao, B. Shim, A. L. Gaeta, M. Tarazkar, D. A. Romanov, R. J. Levis, J. A. Gaffney, M. Foord, S. B. Libby, A. Jaron-Becker, A. Becker, L. Plaja, M. M. Murnane, H. C. Kapteyn, and T. Popmintchev, "Ultraviolet surprise: efficient soft x-ray high-harmonic generation in multiply ionized plasmas," Science **350**, 1225–1231 (2015).
63. I. J. Sola, E. Mével, L. Elouga, E. Constant, V. Strelkov, L. Poletto, P. Villoresi, E. Benedetti, J.-P. Caumes, S. Stagira, C. Vozzi, G. Sansone, and M. Nisoli, "Controlling attosecond electron dynamics by phase-stabilized polarization gating," Nat. Phys. **2**, 319–322 (2006).
64. E. A. J. Marcatili and R. A. Schmeltzer, "Hollow metallic and dielectric waveguides for long distance optical transmission and lasers," Bell Syst. Tech. J. **43**, 1783–1809 (1964).
65. W. Chao, B. D. Harteneck, J. A. Liddle, E. H. Anderson, and D. T. Attwood, "Soft X-ray microscopy at a spatial resolution better than 15 nm," Nature **435**, 1210–1213 (2005).
66. M. D. Seaberg, B. Zhang, D. F. Gardner, E. R. Shanblatt, M. M. Murnane, H. C. Kapteyn, and D. E. Adams, "Tabletop nanometer extreme ultraviolet imaging in an extended reflection mode using coherent Fresnel ptychography," Optica **1**, 39–44 (2014).
67. C. Wagner and N. Harned, "EUV lithography: lithography gets extreme," Nat. Photonics **4**, 24–26 (2010).
68. G. Tallents, E. Wagenaars, and G. Pert, "Lithography at EUV wavelengths," Nat. Photonics **4**, 809–811 (2010).
69. A. Sukhov and J. Berakdar, "Local control of ultrafast dynamics of magnetic nanoparticles," Phys. Rev. Lett. **102**, 057204 (2009).